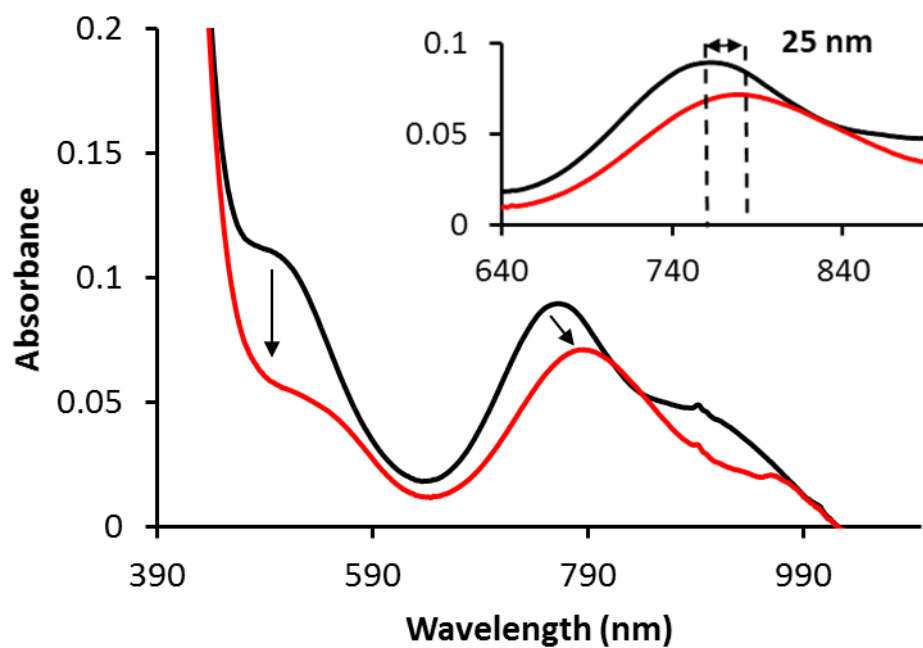
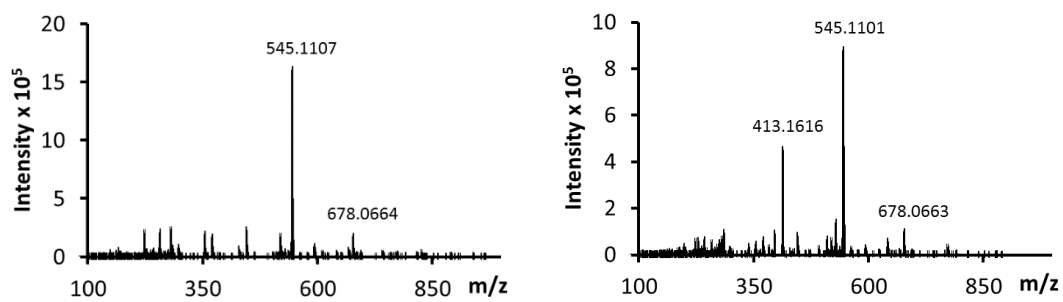


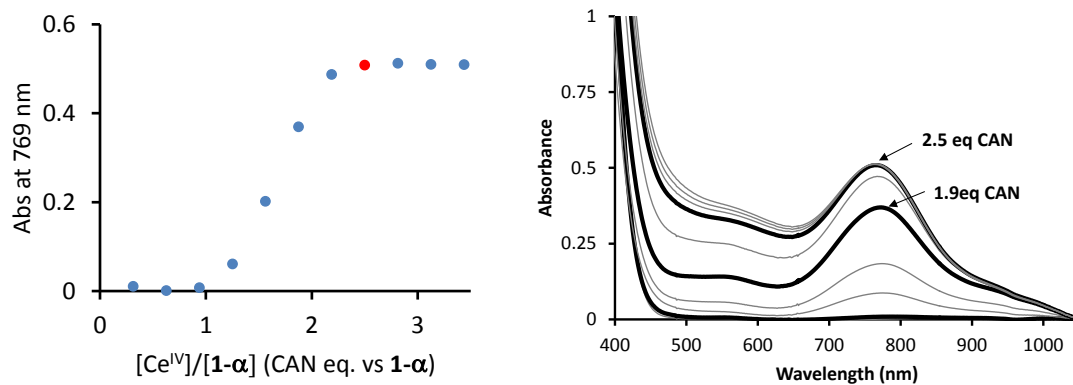
Supplementary Figure 1. UV-Vis spectroscopy of the Fe^{IV}=O species. UV-Vis spectra for **2- α** (left) and **2- β** (right) formed by reaction of **1- α** and **1- β** with CAN (3 eq), (1 mM in Milli-Q water, at pH 1).



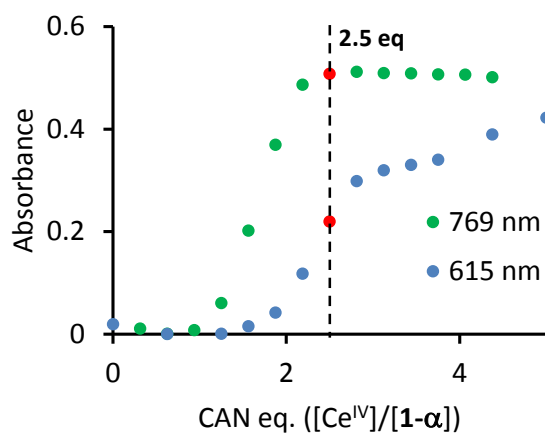
Supplementary Figure 2. Labile ligand exchange on $\text{Fe}^{\text{IV}}=\text{O}$ species. β - $[\text{Fe}^{\text{IV}}(\text{O})(\text{NCCH}_3)(\text{mcp})]^{2+}$ (**2- β**) (black line, $\lambda_{\text{max}} = 753$ nm) was prepared by the addition of 6 eq of CAN to β - $[\text{Fe}^{\text{II}}(\text{mcp})(\text{OTf})_2]$ (1 mM in CH_3CN). β - $[\text{Fe}^{\text{IV}}(\text{O})(\text{H}_2\text{O})(\text{mcp})]^{2+}$ (red line, $\lambda_{\text{max}} = 778$ nm) was obtained by the addition of 1000 equiv. of water to β - $[\text{Fe}^{\text{IV}}(\text{O})(\text{NCCH}_3)(\text{mcp})]^{2+}$. Inset, magnification of the shift observed in the 640 – 900 nm range.



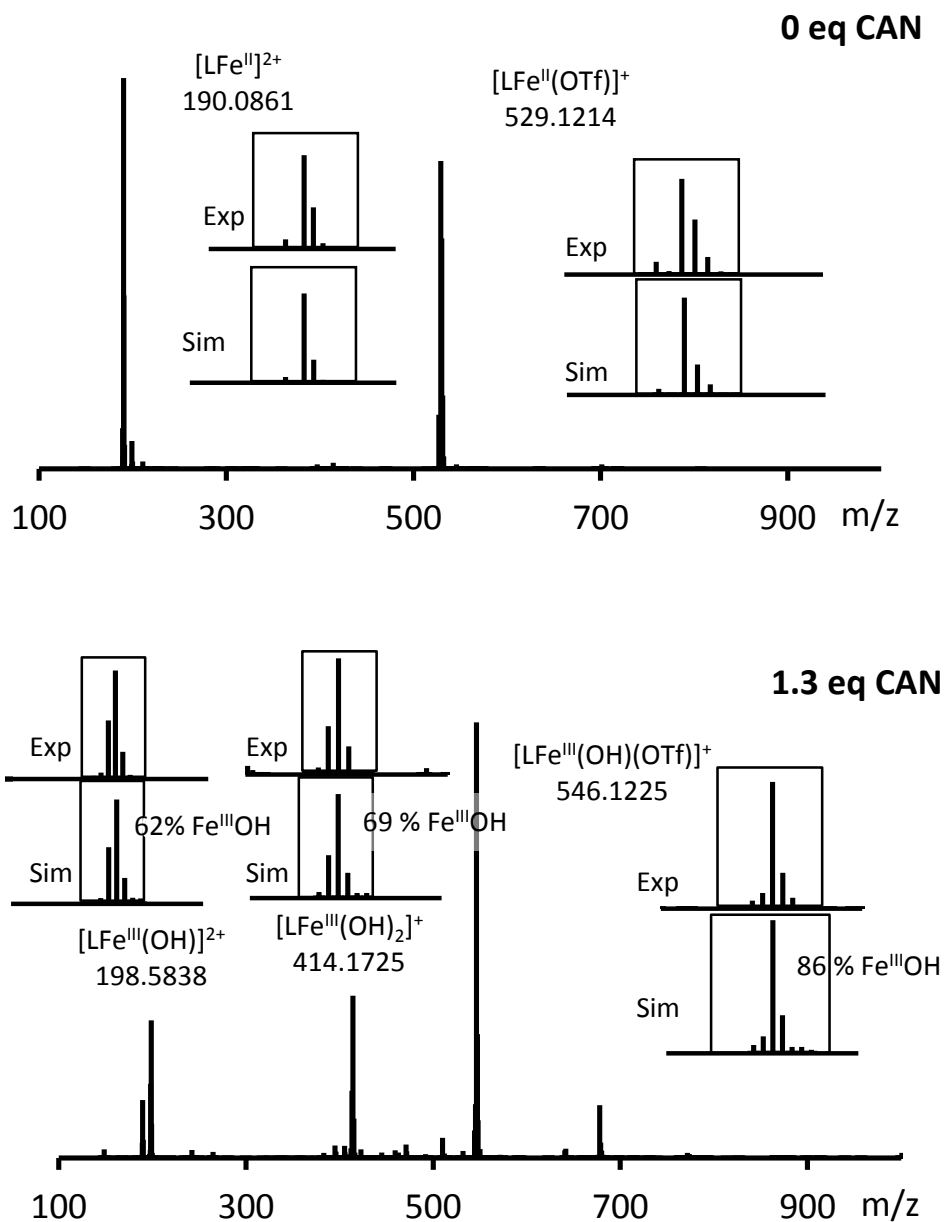
Supplementary Figure 3. High resolution mass spectrometry of the $\text{Fe}^{\text{IV}}=\text{O}$ species. CSI-HRMS spectra recorded immediately after the addition of 50 μL of CAN (3 mM in HOTf:H₂O 3:10) to 1 mM solutions of **1-β** (left) or **1-α** (right) in MilliQ water (2 mL).



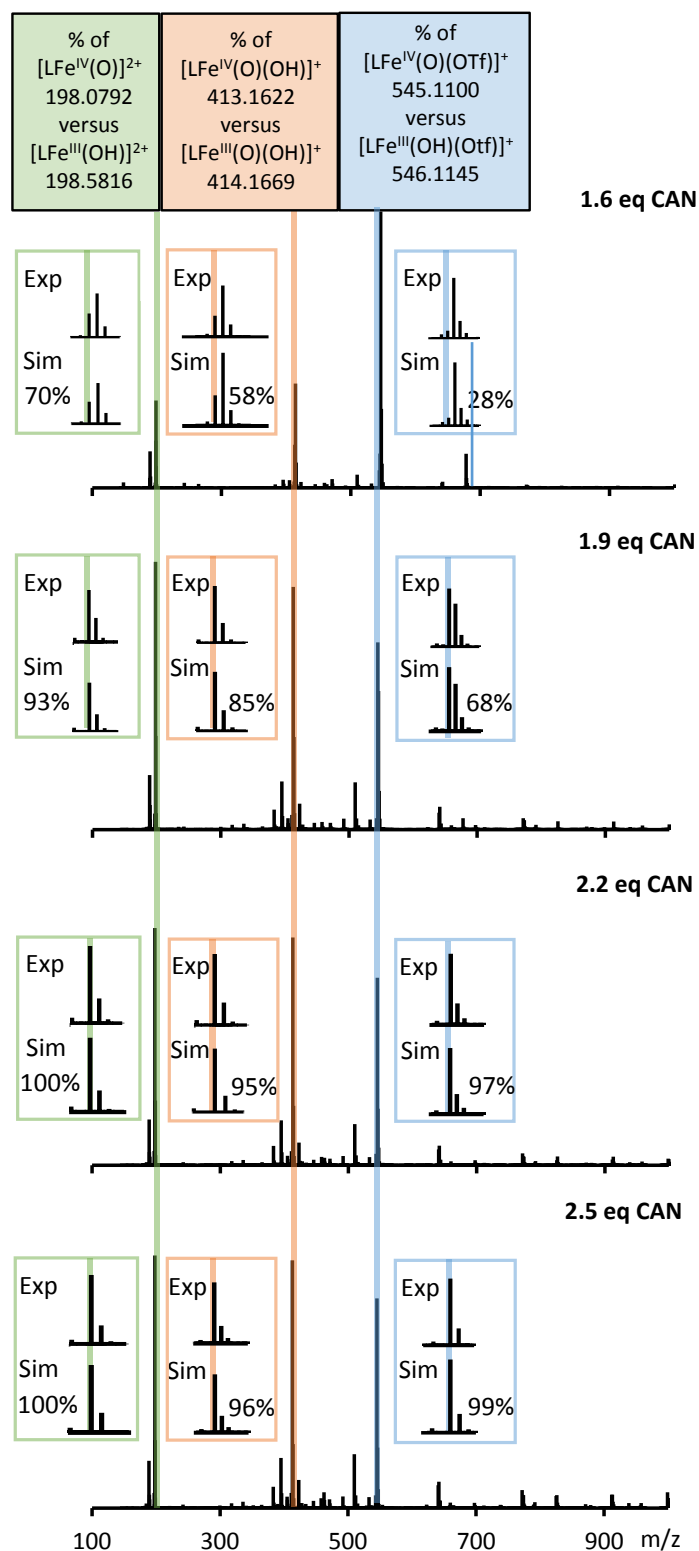
Supplementary Figure 4. Titration of 1- α with Ce(IV) monitored by UV-Vis. Titration of 1- α (5mM) with 0 – 3 eq of CAN at -8 °C in MeCN:H₂O (1:1) at pH 1. Highlighted in red is the abs at 2.5 eq of CAN for the λ_{max} corresponding to the Fe^{IV}O feature ($\lambda_{\text{max}}=769$ nm).



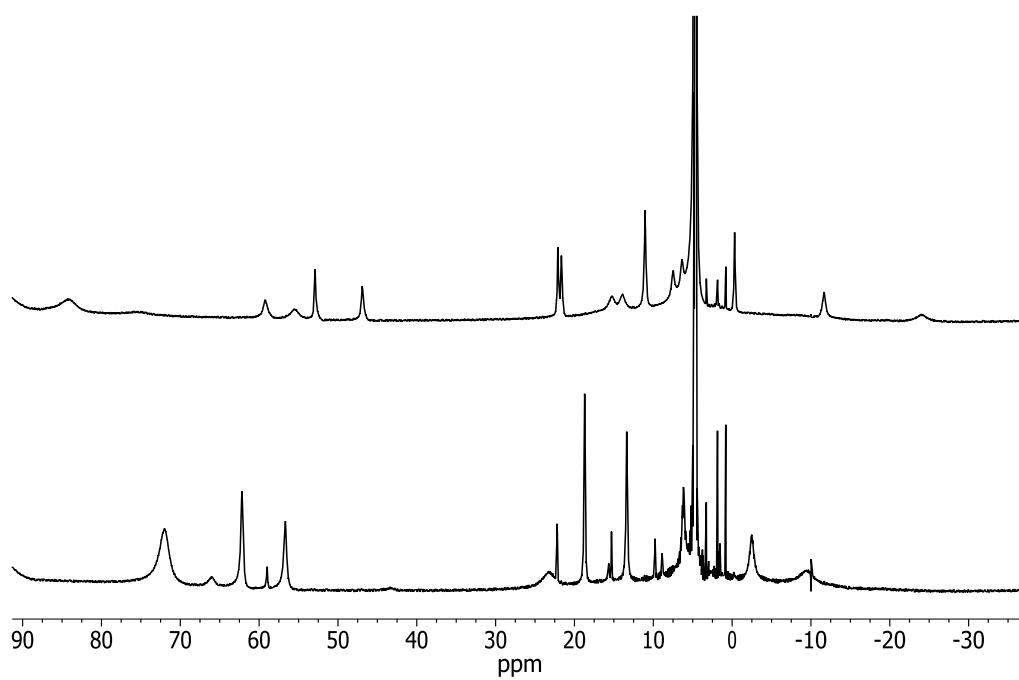
Supplementary Figure 5. Titration of 1- α with Ce(IV) monitored by UV-Vis at 769 and 615 nm. Titration of 1- α (5 mM) with 0 – 5 eq of CAN at -8 °C in MeCN:H₂O (1:1) at pH 1. Highlighted in red is the absorbance after the addition of 2.5 eq of CAN at λ_{max} corresponding to the 2- α feature (λ_{max} = 769 nm, left) and for the λ_{max} corresponding to 3- α (λ_{max} = 615 nm, left).



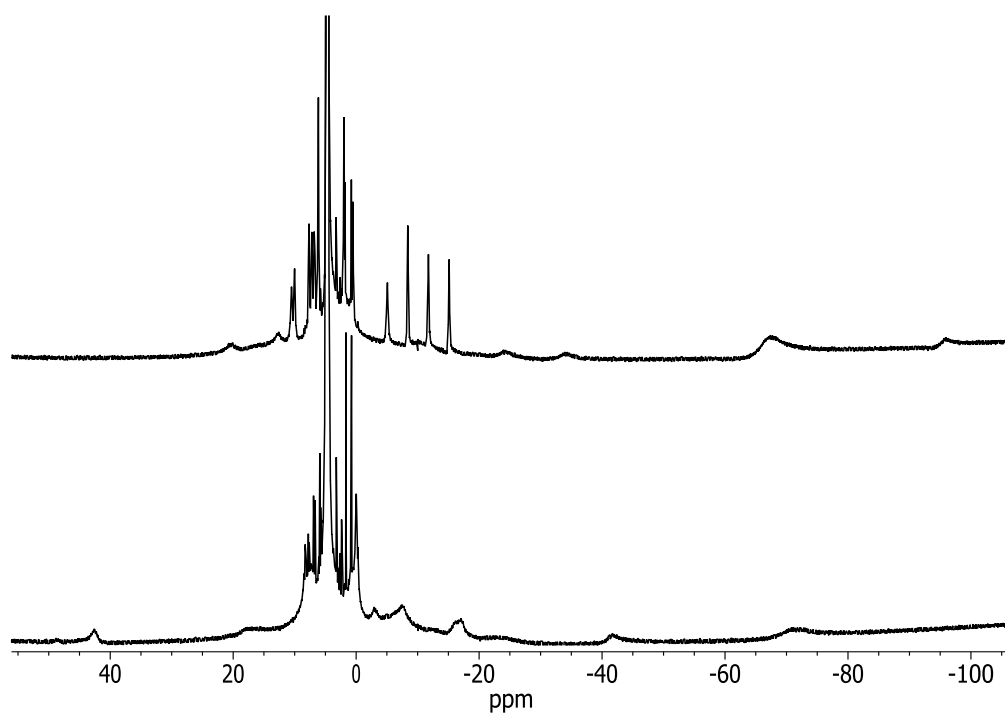
Supplementary Figure 6. Titration of 1- α with Ce(IV) monitored by HRMS. HRMS spectrum of **1 α** (5mM) in MeCN:H₂O (1:1, -8°C) before and after the addition of 1.3 equiv. of CAN. Inset shows magnifications of the isotopic patterns along with the simulated spectra. Percentages represent the fraction of Fe^{III} in a mixture of Fe^{III} and Fe^{IV} species in the simulated pattern.



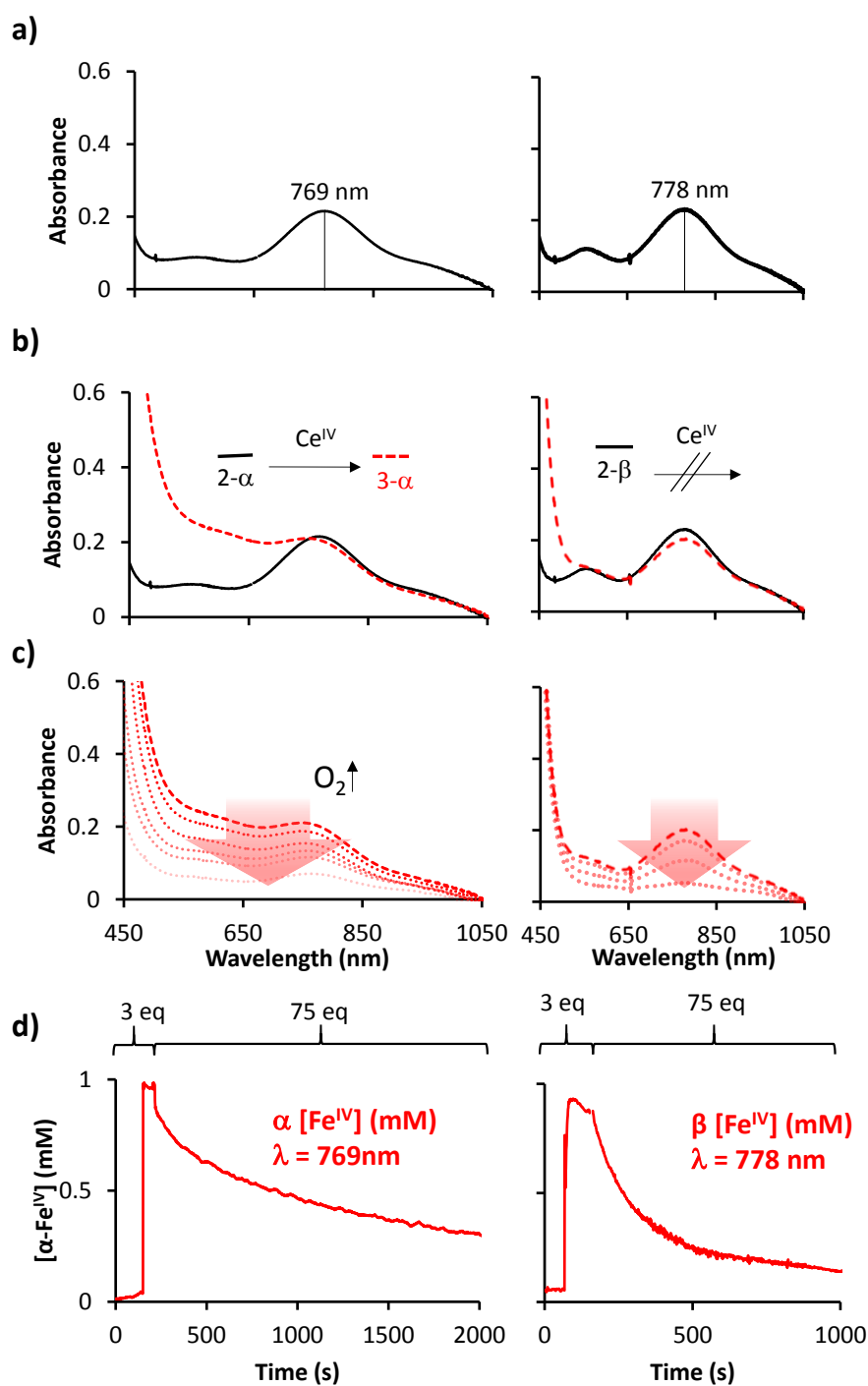
Supplementary Figure 7. Titration of 1- α with Ce(IV) monitored by HRMS. HRMS spectra of **1 α** (5mM) in MeCN:H₂O (1:1, -8 °C) after the addition of increasing amounts of CAN. Inset shows magnifications of the isotopic patterns along with the simulated spectra. Percentages represent the fractions of Fe^{IV} in a mixture of Fe^{III} and Fe^{IV} species in the simulated patterns.



Supplementary Figure 8. ¹H-NMR spectroscopy of the Fe^{II} species. ¹H-NMR spectra of **1-β** (top, 4.5 mM) and **1-α** (bottom, 4.5 mM) in D₂O at 5 °C.

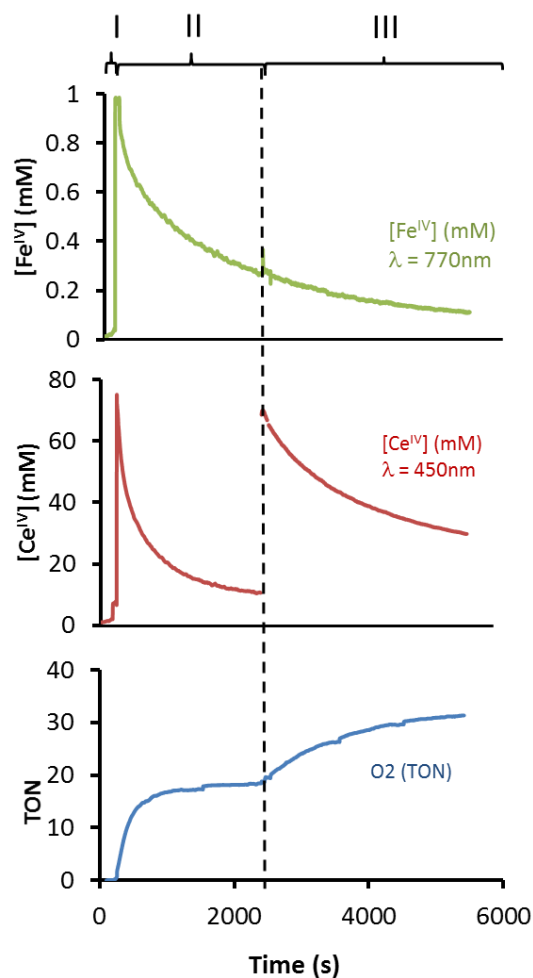


Supplementary Figure 9. ¹H-NMR spectroscopy of the Fe^{IV} species. ¹H-NMR spectra of **2-β** (top, 4.5 mM) and **2-α** (bottom, 4.5 mM) in D₂O at 5 °C generated by adding 3 eq of CAN (50 μL, final pH = 1).

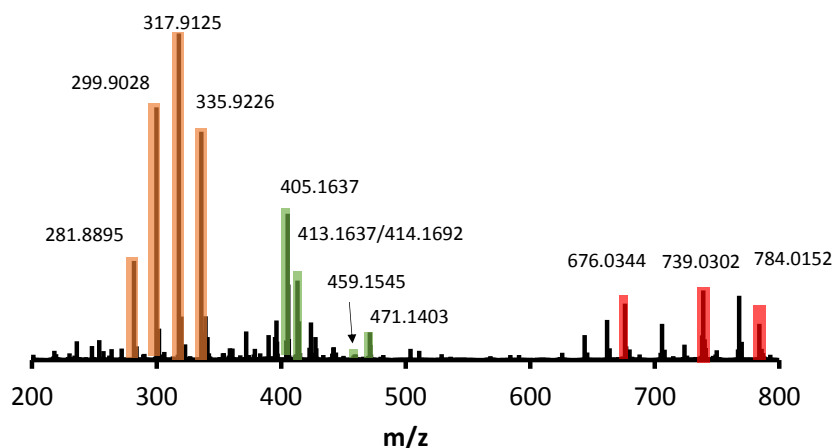


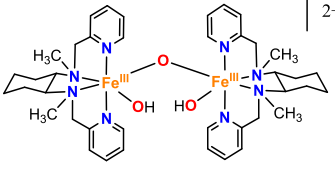
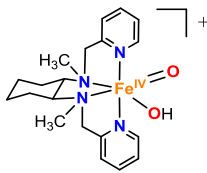
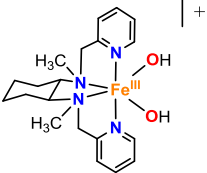
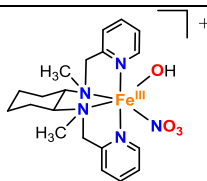
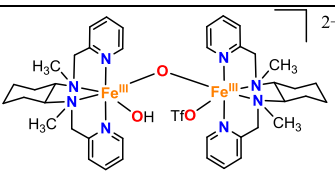
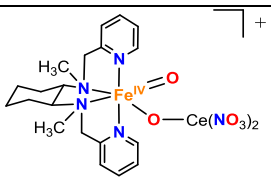
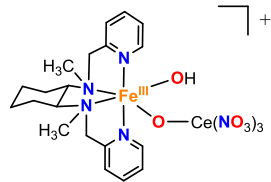
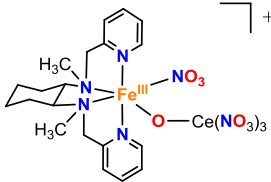
Supplementary Figure 10. Study of the catalytically active species by UV-Vis spectroscopy.

a) UV-Vis spectra of **2-α** (left) and **2-β** (right) generated by the addition of 3 equiv. of CAN to an aqueous solution of **1-α** and **1-β** (1 mM) at 25 °C, respectively. **b)** Spectra recorded immediately after the addition of 75 equiv. of CAN to **2-α** (left) and **2-β** (right) and **c)** its time evolution. **d)** Traces of the 769 nm and 778 nm band, corresponding to **2-α** and **2-β**, upon addition of (3 + 75) eq of CAN to **1-α** and **1-β** respectively.

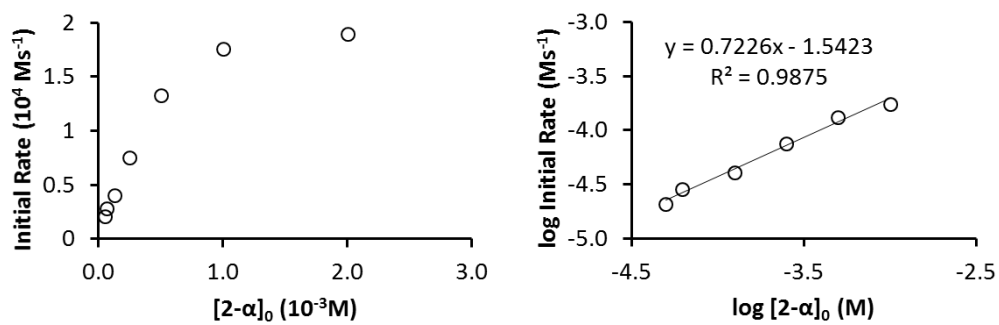


Supplementary Figure 11. Real-time manometry/UV-Vis monitoring of oxygen evolution and cerium(IV) consumption. Oxygen evolution (blue, bottom), Ce^{IV} consumption (red, middle) and $\text{Fe}^{\text{IV}}=\text{O}$ disappearance (green, top) monitored by a pressure transducer coupled with a UV-Vis spectrometer for **1- α** , (I) on the addition of 3 eq. of Ce^{IV} to fully form the $\text{Fe}^{\text{IV}}=\text{O}$ species and (II), after the addition of 75 eq. of Ce^{IV} . Kinetic traces for $[\text{Ce}(\text{IV})]$ and **2- α** were monitored at 450 nm and 769 nm, respectively. $\Delta[\text{O}_2](\text{TON})$ was monitored by a pressure transducer. (III) After 2300 s, 75 eq of Ce^{IV} were added to the solution.

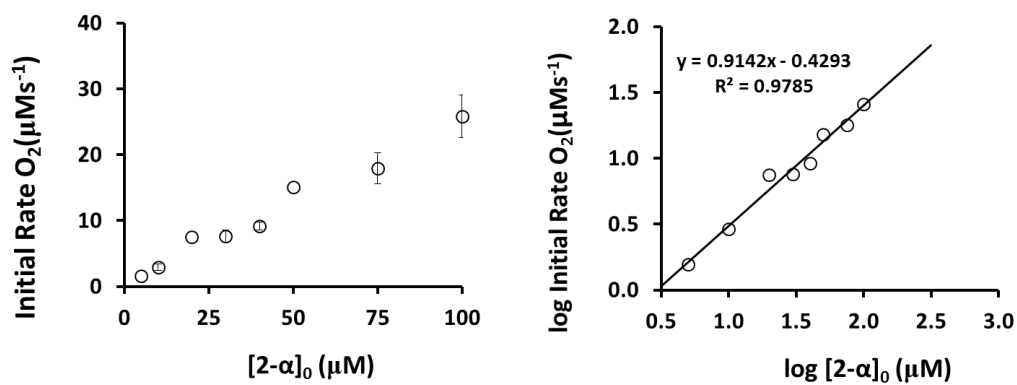


 <p> Sim. 405.1665 (810.3331) Exp. H₂O 405.1637 Exp. D₂O 406.1728 Exp. H₂¹⁸O 408.1732 </p>	 <p> Sim. 413.1634 Exp. H₂O 413.1627 Exp. D₂O 414.1703 Exp. H₂¹⁸O 417.1720 </p>	 <p> Sim. 414.1718 Exp. H₂O 414.1692 Exp. D₂O 416.1848 Exp. H₂¹⁸O 418.1764 </p>
 <p> Sim. 459.1569 Exp. H₂O 459.1545 Exp. D₂O 460.1628 Exp. H₂¹⁸O 461.1556 </p>	 <p> Sim. 471.1406 (942.2824) Exp. H₂O 471.1403 Exp. D₂O 471.6453 Exp. H₂¹⁸O 473.1459 </p>	 <p> Sim. 676.0367 Exp. H₂O 676.0353 Exp. D₂O 676.0369 Exp. H₂¹⁸O 680.0444 </p>
 <p> Sim. 739.0329 Exp. H₂O 739.0302 Exp. D₂O 740.0339 Exp. H₂¹⁸O 743.0398 </p>	 <p> Sim. 784.0180 Exp. H₂O 784.0147 Exp. D₂O 784.0191 Exp. H₂¹⁸O 786.0214 </p>	

Supplementary Figure 12. HRMS analysis of the decomposition products. Positive mode HRMS recorded after complete decay of **3-*a*** formed by addition of CAN (75 eq.) to [Fe(OTf)₂(mcp)] (1 mM) in Milli-Q H₂O. Peaks highlighted in orange are derived from the cerium since they are present in the blank CAN HRMS experiments, in green are monomeric iron species and in red Fe-Ce heterobimetallic species. Labelled and non-labelled m/z values for the main species are included in the table below.

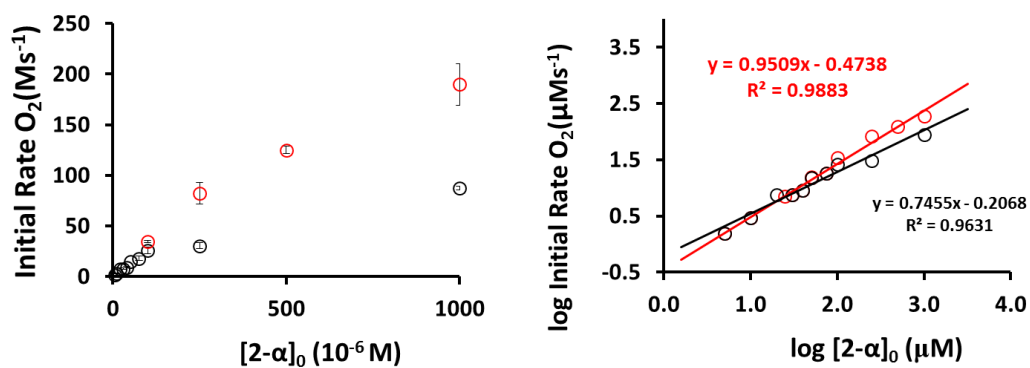


Supplementary Figure 13. Initial rates of Ce^{IV} consumption with different amounts of catalyst. Left) Plot of initial rates for Ce^{IV} consumption versus $[2-\alpha]_0$ in H_2O at $\text{pH} = 1$ and 25°C : $[2-\alpha]_0 = 0.05 - 2 \text{ mM}$; $[\text{Ce}^{\text{IV}}]_0 = 18.75 \text{ mM}$. Right) Log-log plot in the determination of reaction order for $2-\alpha$ ($\text{Fe}^{\text{IV}}=\text{O}$).



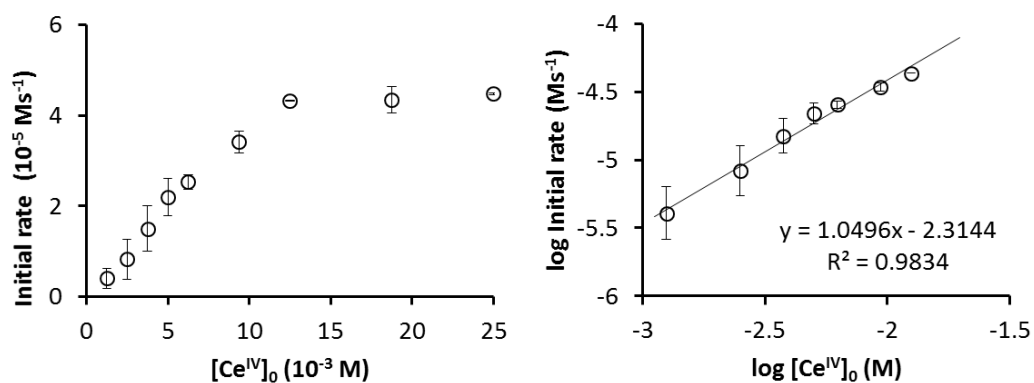
Supplementary Figure 14. Initial rates of O₂ evolution with different amounts of catalyst.

Reaction order under optimized catalytic conditions. Left) initial rates of O₂ evolution versus [2-α]₀, in H₂O at pH = 0.8 and 25 °C: [2-α]₀ = 5 – 100 μM; [Ce^{IV}]₀ = 125 mM. Right) Log-log plot in the determination of reaction order for 2-α (Fe^{IV}=O).

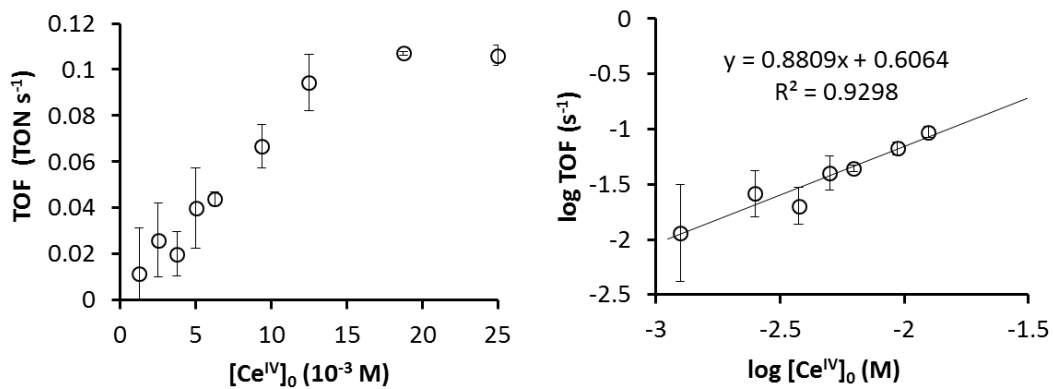


Supplementary Figure 15. Comparison between manometry and by UV-Vis spectroscopy.

Reaction order vs $[2-\alpha]$. In red $[Ce^{IV}]_0 = 500$ mM, and in black, $[Ce^{IV}]_0 = 125$ mM. Left) In black, initial rates of O₂ evolution versus $[2-\alpha]_0$, in H₂O at pH = 0.8 and 25 °C: $[2-\alpha]_0 = 5 - 1000$ μM; $[Ce^{IV}]_0 = 125$ mM; In red, $[Ce^{IV}]_0 = 500$ mM.(pH 0.6) Right) Log-log plot in the determination of reaction order for $2-\alpha$ ($Fe^{IV}=O$).

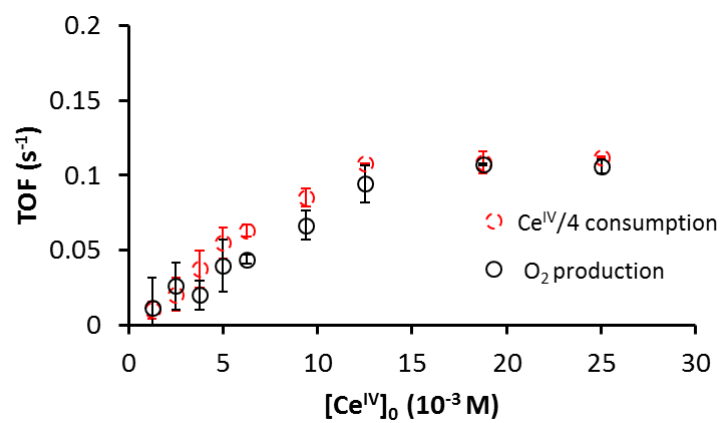


Supplementary Figure 16. Initial rates of Ce^{IV} consumption with different amounts of Ce^{IV} . Left) initial rates of Ce^{IV} consumption versus $[\text{Ce}^{\text{IV}}]_0$, in H_2O $\text{pH} = 1$ at 25°C : $[\mathbf{2-a}]_0 = 0.1 \text{ mM}$; $[\text{Ce}^{\text{IV}}]_0 = 1.25 - 18.75 \text{ mM}$. Right) Log-log plot in the determination of reaction order for Ce^{IV} .



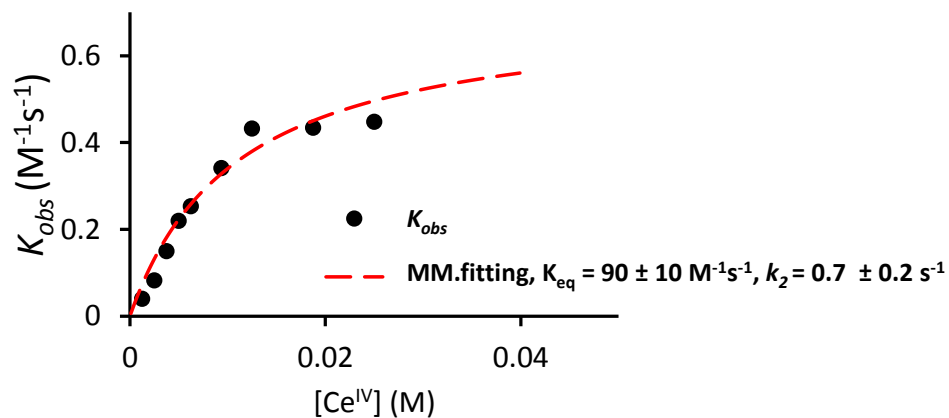
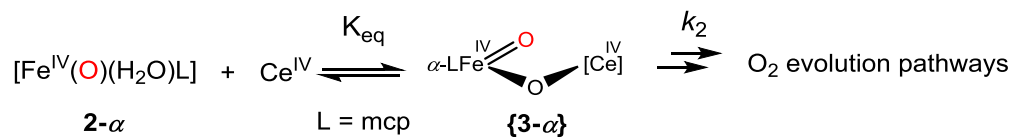
Supplementary Figure 17. Initial rates of O₂ evolution with different amounts of Ce^{IV}.

Left) initial rates of O₂ evolution versus [Ce^{IV}]₀, in H₂O pH = 1 at 25 °C: [2-**a**]₀ = 0.1 mM; [Ce^{IV}]₀ = 1.25 – 18.75 mM. Right) Log-log plot in the determination of reaction order for Ce.

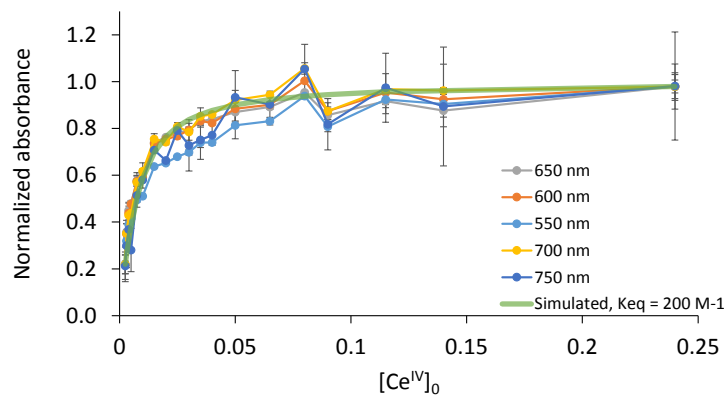


Supplementary Figure 18. Comparison between manometry and by UV-Vis spectroscopy.

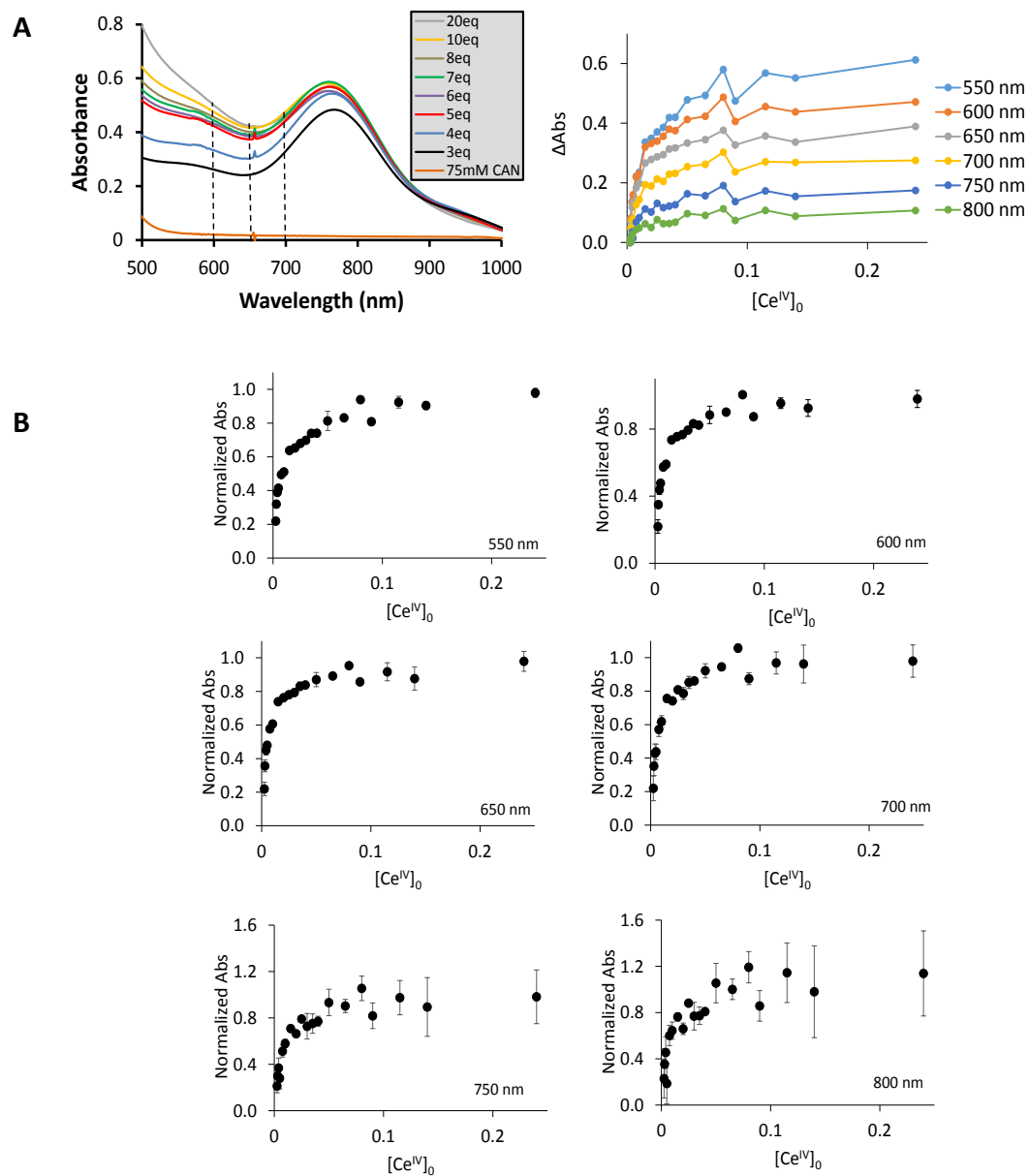
Initial rates of O₂ evolution (circles, black) and [Ce^{IV}]/4 consumption (squares, red) versus [Ce^{IV}]₀.



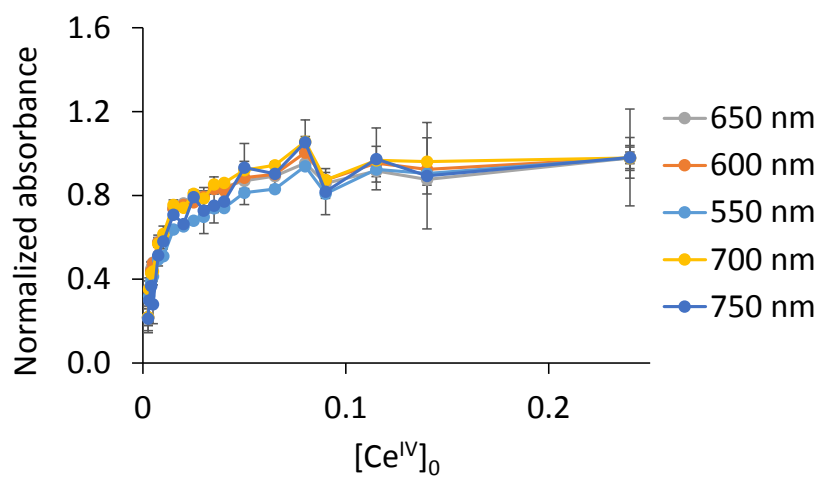
Supplementary Figure 19. Estimation of the pre-equilibrium constant. Initial rates of Ce^{IV} consumption versus $[Ce^{\text{IV}}]_0$ (black spots) and the superimposed fitting derived from the Michaelis-Menten model (red dashed line). Conditions: H_2O , $\text{pH} = 1$, 25°C , $[\mathbf{2-\alpha}]_0 = 0.1 \text{ mM}$; $[Ce^{\text{IV}}]_0 = 1.25 - 18.75 \text{ mM}$.



Supplementary Figure 20. Starting point for the determination of K_{eq} . Experimental data and a simulated [Abs vs Ce] curve using a value of 200 M^{-1} for the K_{eq} (starting value for the iterative calculation). Normalized absorbance is employed. Vertical bars represent the errors associate to triplicate repetitions

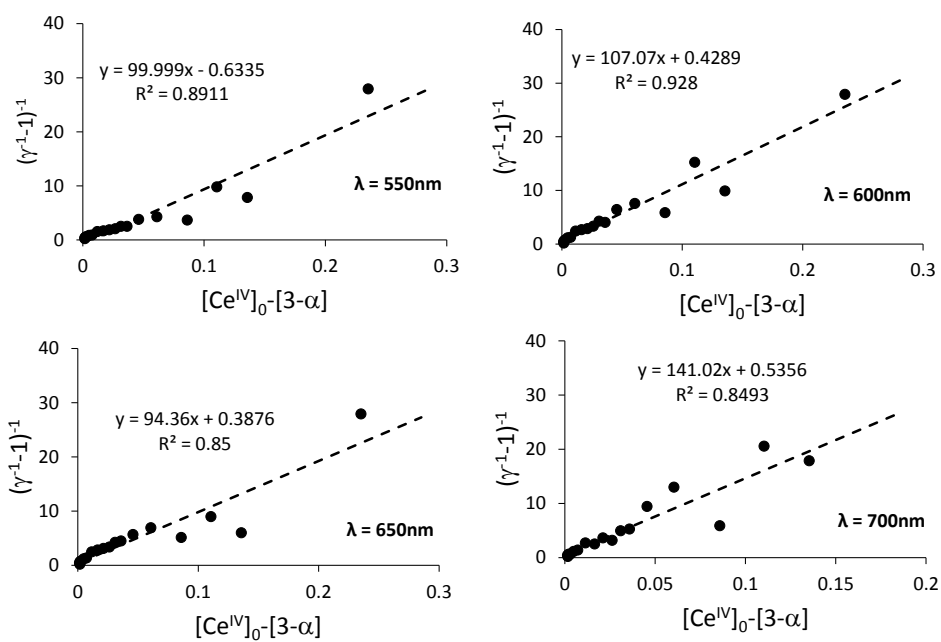


Supplementary Figure 21. Titration curves at different wavelengths. Titration of 2- α (5.0 mM, path length 0.5 cm) with CAN (5-90 mM) at pH 1 in H₂O:MeCN (1:1 v/v) at 265 K. **A**) UV-Vis spectra (left) and absorbance at λ values of 550, 600, 650, 700, 750, 800 nm (right) versus $[Ce^{IV}]$. **B**) Normalized absorbance for the at λ values of 550, 600, 650, 700, 750, 800 nm (right) versus $[Ce^{IV}]$. Vertical bars represent the errors associate to triplicate repetitions.

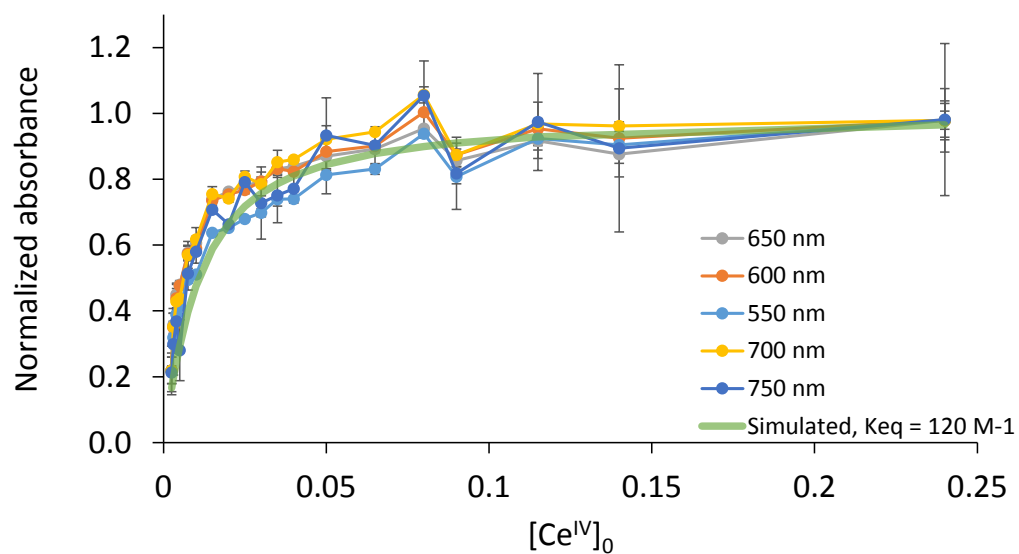


Supplementary Figure 22. Overlapping of the titration curves at different wavelengths.

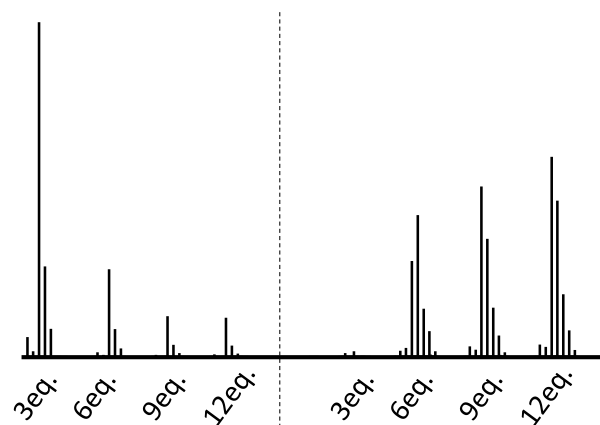
Comparison between the normalized absorbance for the at λ values of 550, 600, 650, 700, 750 nm (right) versus [Ce^{IV}]. Vertical bars represent the errors associate to triplicate repetitions.



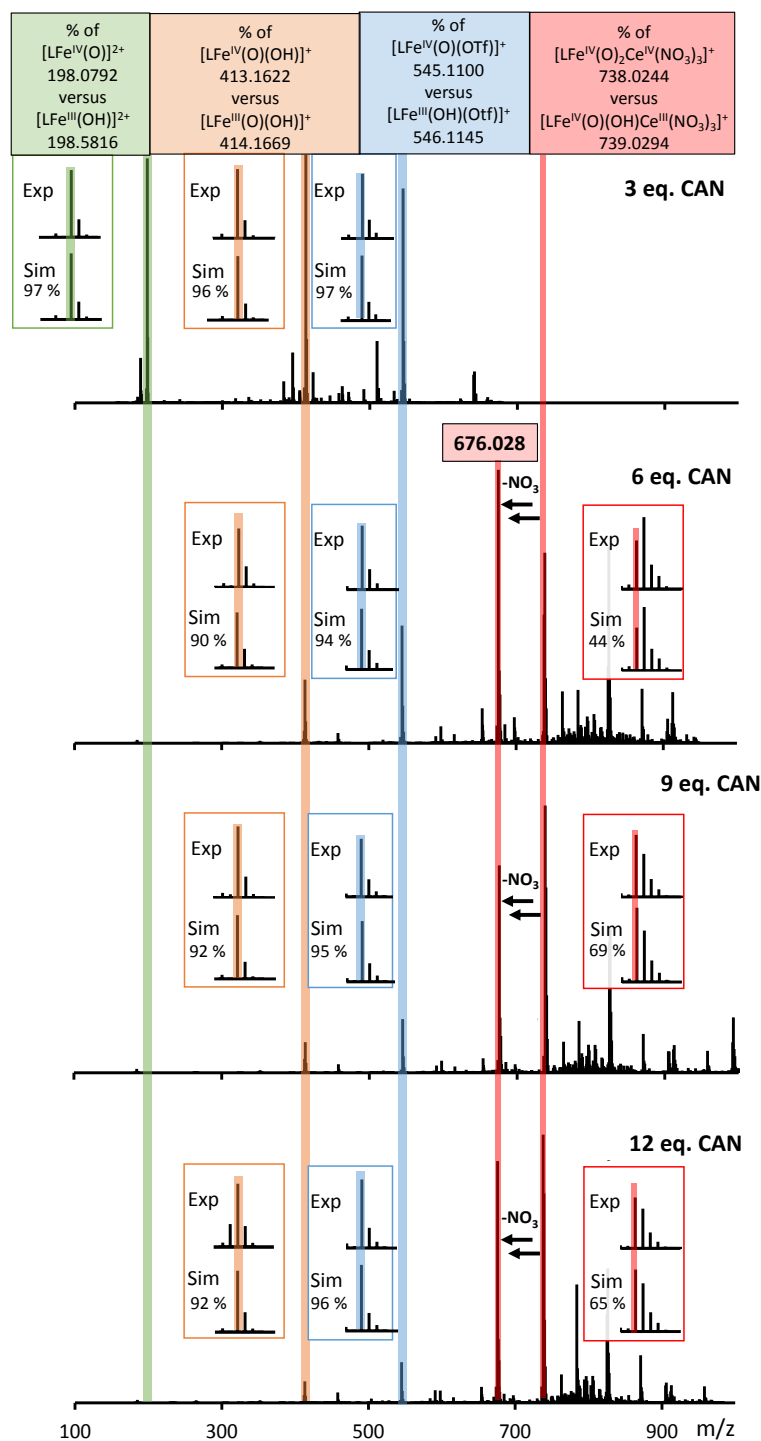
Supplementary Figure 23. Linearization of the titration curves. Comparison between $(\gamma^{-1}-1)^{-1}$ vs $[\text{Ce}^{\text{IV}}]_0 - [3-\alpha]$ fittings at different wavelengths (550, 600, 650 and 700 nm).



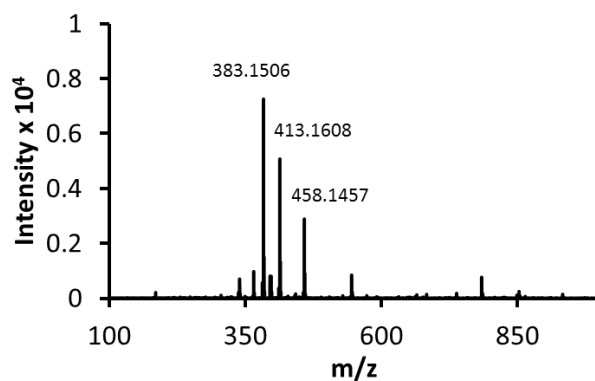
Supplementary Figure 24. Overlapping of the K_{eq} calculated using the iterative method and the experimental data. Comparison between the normalized absorbance for the at λ values of 550, 600, 650, 700, 750, 800 nm (right) versus $[Ce^{IV}]_0$. Vertical bars represent the errors associate to triplicate repetitions.



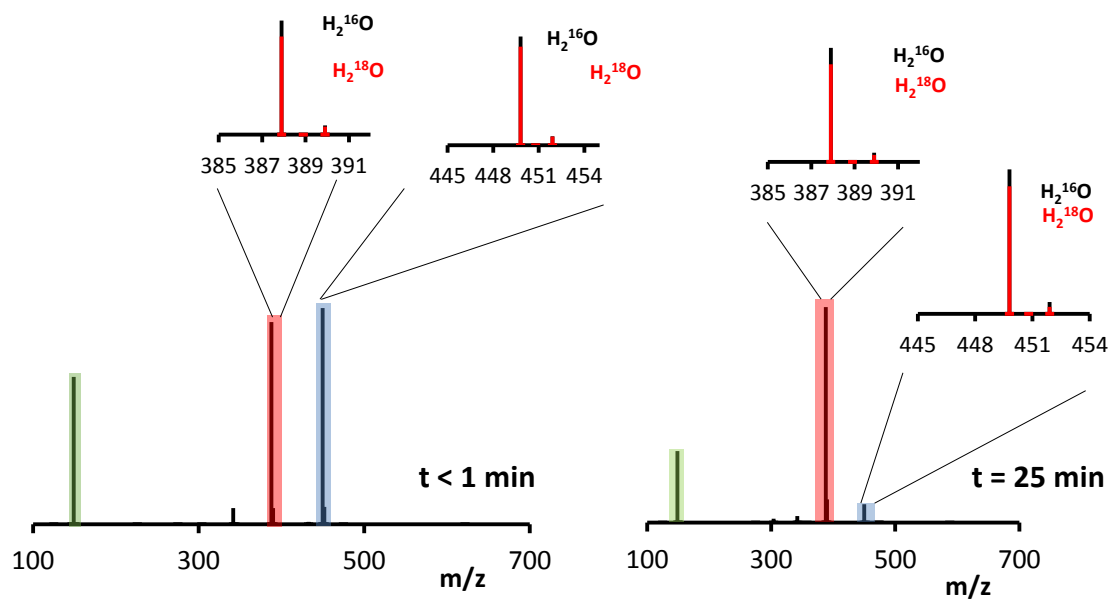
Supplementary Figure 25. HRMS titration of 1- α with Ce^{IV}. Peak intensities of **2- α** (left, [(mcp)Fe^{IV}(O)(OTf)], 545.1133 m/z) and **3- α** (right, 738.0251 m/z) after the addition of different amounts of CAN. Conditions: 1 mM on **1- α** , -8 °C.



Supplementary Figure 26. Analysis of the species generated during HRMS titration of 1- α with Ce^{IV}. HRMS spectrum of **1- α** (5 mM) in MeCN:H₂O (1:1, -8°C) after the addition of increasing amounts of CAN. Inset shows magnifications of the isotopic patterns along with the simulated spectra. Percentages represent. The HRMS peak at 676.0282 m/z corresponds to the loss of neutral NO₃ from **3- α** . Peaks prominent at 784.0150 and 824.9906 m/z correspond to [**3- α**]+NO₃-O and [**3- α**]+NO₃+CN₃CN-O, respectively.

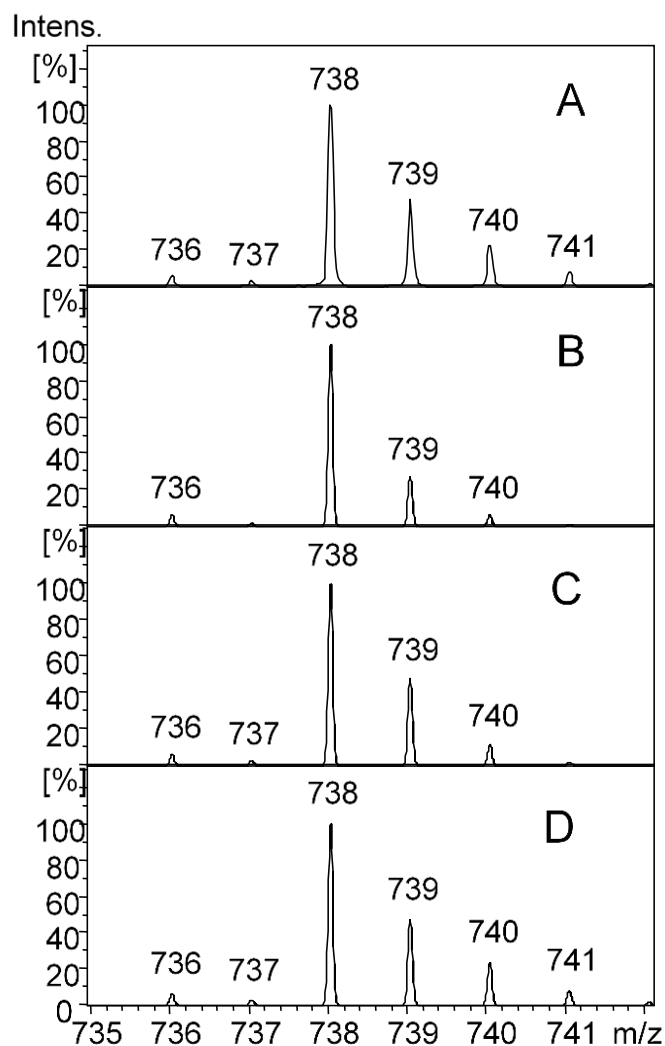


Supplementary Figure 27. HRMS of the oxidation of 1- β . CSI-HRMS spectrum recorded immediately after the addition of 75 eq of CAN to an aqueous solution of **1- β** (1 mM), using a cryospray probe coupled with a TOF analyzer (dry gas and nebulizer gas temperatures were set at 25 °C). The most intense peaks correspond to $[\text{Fe}^{\text{IV}}\text{O}(\text{OH})(\text{mcp})]^+$ (413.1627 m/z) and $[\text{Fe}^{\text{IV}}(\text{O})(\text{NO}_3)(\text{mcp})]^+$ (458.1463 m/z).

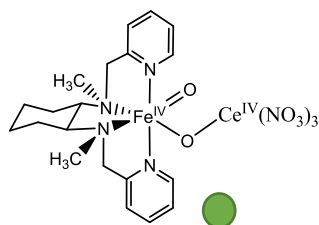
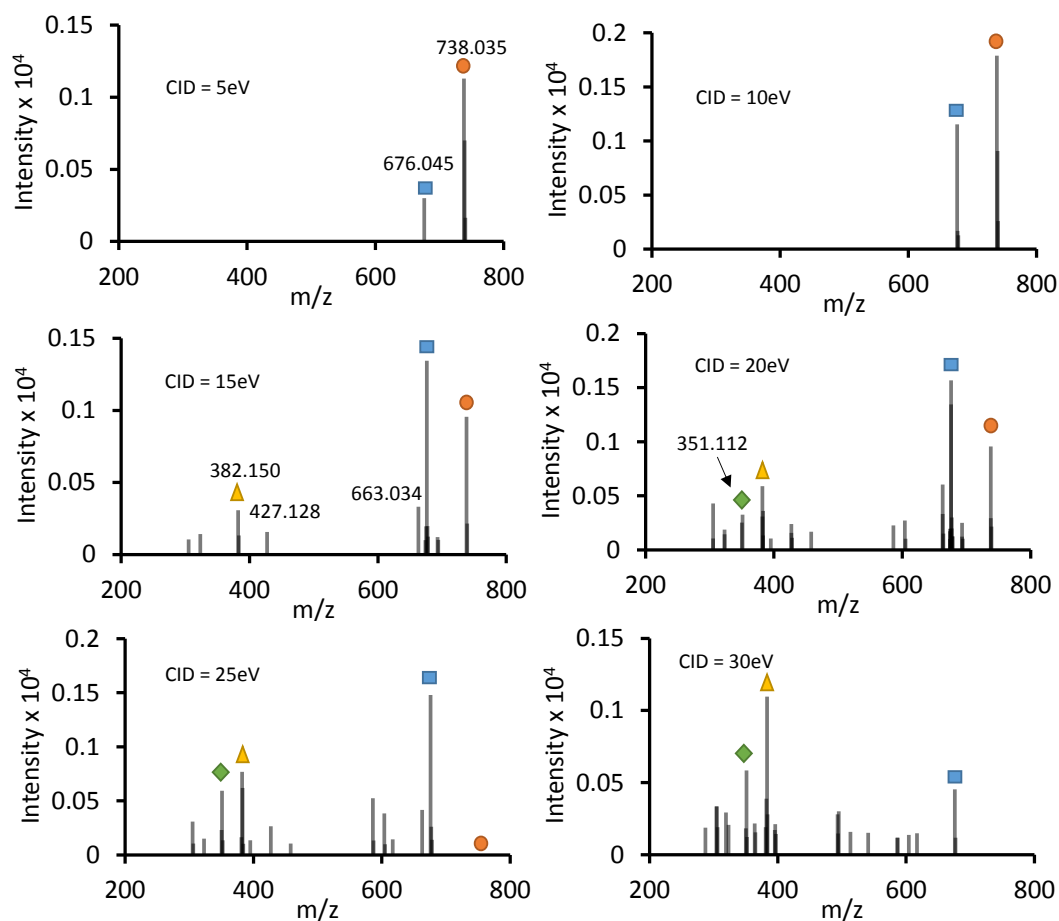


Species	Exp (m/z)	Theo (m/z)
$[\text{Ce}^{\text{IV}}(\text{NO}_3)_5]^-$	449.8496	449.8451
$[\text{Ce}^{\text{III}}(\text{NO}_3)_4]^-$	387.8610	387.8573
$[\text{OTf}]^-$	148.9543	148.9520

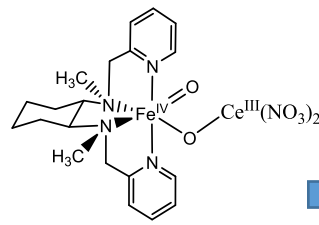
Supplementary Figure 28. Negative-mode HRMS analysis. Negative mode HRMS recorded immediately (< 1min, left) and 25 min (right) after the addition of CAN (75 eq.) to $[\text{Fe}(\text{OTf})_2(\text{mcp})]$ (0.5 mM) in Milli-Q H_2O (magnification, black spectra) and 98% H_2^{18}O (magnification, red spectra). Labelled and non-labelled m/z values for the main species are included in the table below.



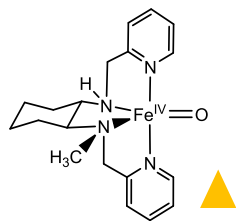
Supplementary Figure 29. HRMS analysis of the isotopic pattern of 3- α . A) Experimental spectrum of 3- α . B) Simulated spectrum of pure $\{[\text{Fe}^{\text{IV}}(\text{O})(\text{mcp})(\mu\text{-O})\text{Ce}^{\text{IV}}(\text{NO}_3)_3]\}^+$ using monoisotopic Ce (139.9). C) Simulated spectrum of a mixture of $\{[\text{Fe}^{\text{IV}}(\text{O})(\text{mcp})(\mu\text{-O})\text{Ce}^{\text{IV}}(\text{NO}_3)_3]\}^+$ (84%) and $\{[\text{Fe}^{\text{III}}(\text{OH})(\text{mcp})(\mu\text{-O})\text{Ce}^{\text{IV}}(\text{NO}_3)_3]\}^+$ (16%) using monoisotopic Ce (139.9). D) Simulated spectrum of pure $\{[\text{Fe}^{\text{IV}}(\text{O})(\text{mcp})(\mu\text{-O})\text{Ce}^{\text{IV}}(\text{NO}_3)_3]\}^+$ using the natural isotope distributions of Fe and Ce.



Chemical Formula: $C_{20}H_{28}CeFeN_7O_{11}$
 Exact Mass: 738.0251
 Monocharged (+4, +4 or +5, +3)

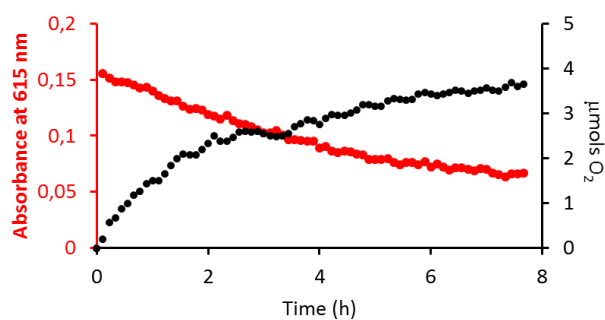


Chemical Formula: $C_{20}H_{28}CeFeN_6O_8$
 Exact Mass: 676.0372
 Monocharged (+4, +3 or +3, +4)



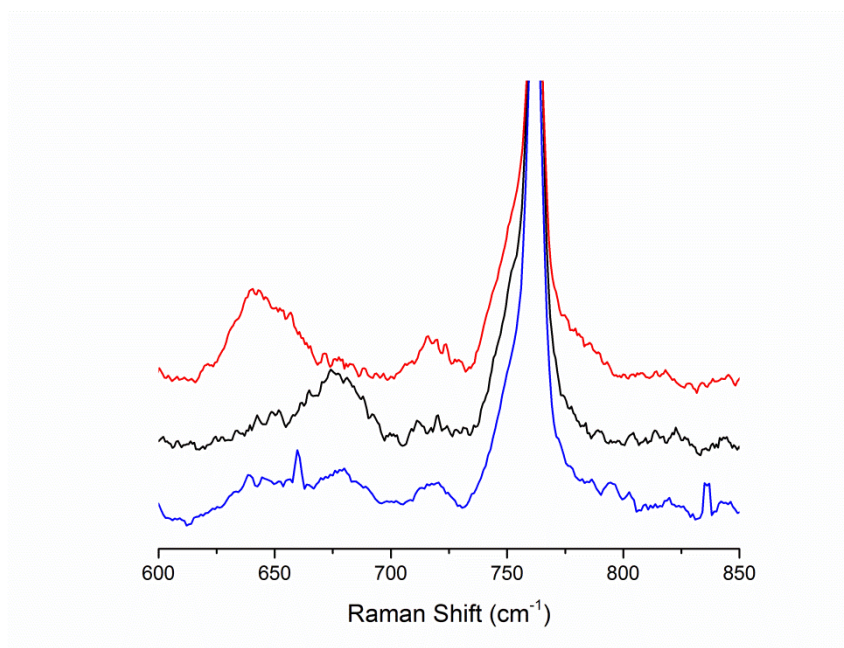
Chemical Formula: $C_{19}H_{26}FeN_4O$
 Exact Mass: 382.1456
 Monocharged (+4)

Supplementary Figure 30. Collision induced HRMS experiments. Effect of the collision-induced dissociation (CID) for the MS/MS spectrum of **3- α** (738.035 m/z). The figure includes the mass spectra (top) and the structure of the most relevant ions detected (bottom).

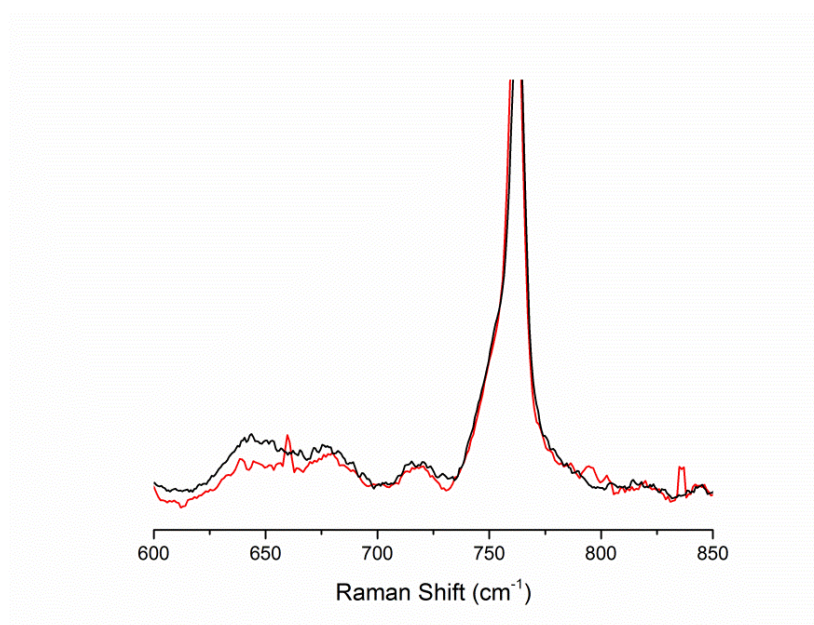


Supplementary Figure 31. Low temperature real-time manometry/UV-Vis monitoring of oxygen evolution and intermediate consumption. Oxygen evolution (black), and **3- α** disappearance (red) monitored by a pressure transducer coupled with a UV-Vis spectrometer for **1- α** , (I) on the addition of 20 eq. of Ce^{IV} to **3- α** species at -8°C in $\text{H}_2\text{O}:\text{CH}_3\text{CN}$ (1:1; v:v). $\Delta[\text{O}_2]$ (TON) was monitored by a pressure transducer.

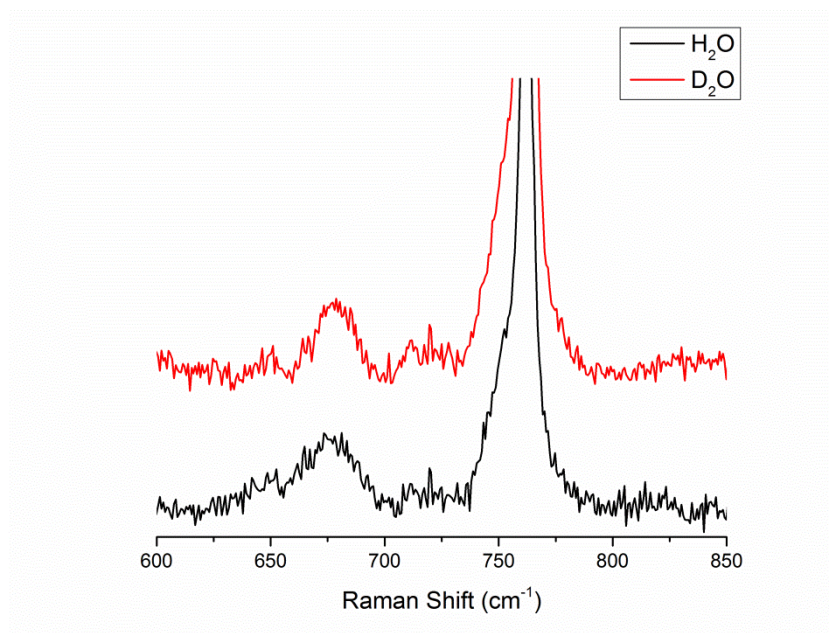
a)



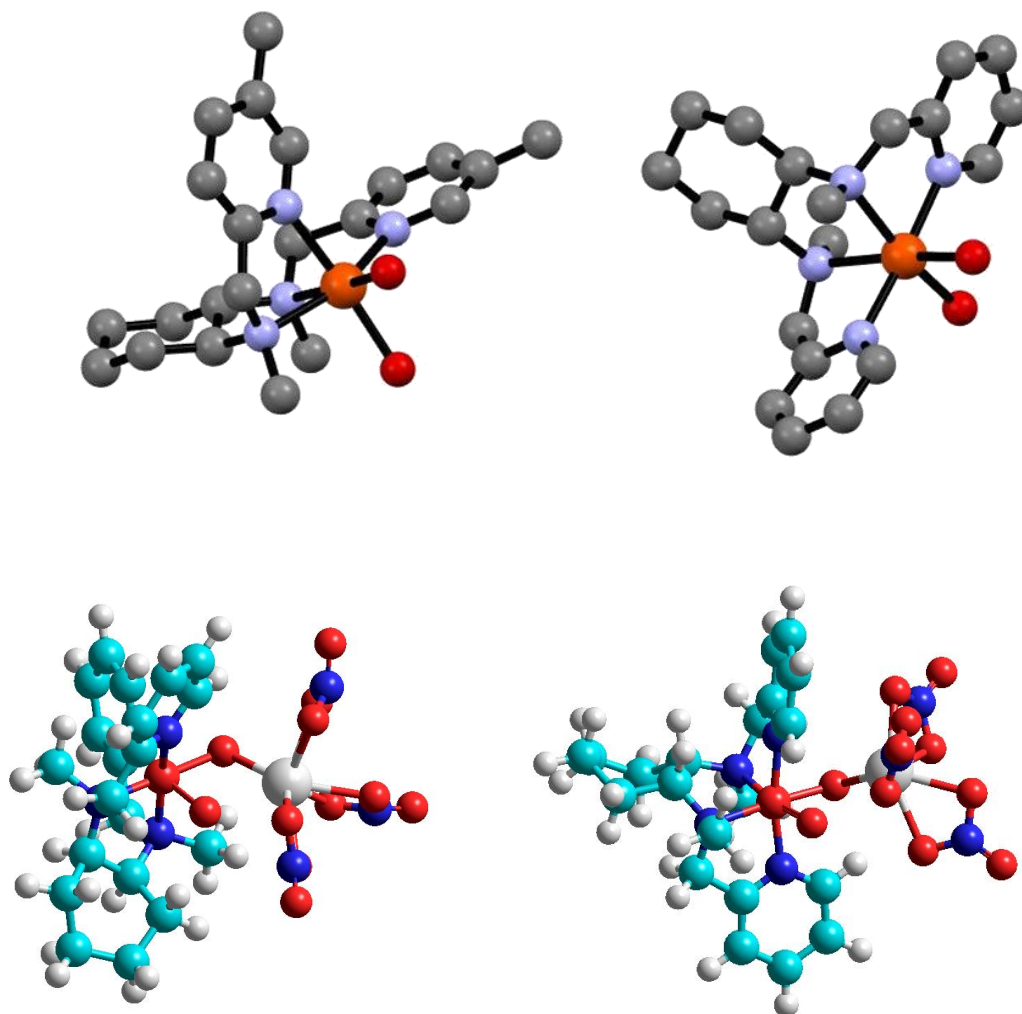
b)



Supplementary Figure 32. Resonance Raman labelling experiments. a) Resonance Raman spectra of **3- α** (λ_{ex} 514.5 nm, 140 mW) prepared upon addition of 9 eq. of CAN to a 6-mM solution of **1- α** in 1:1 H₂O:MeCN. H₂¹⁶O: Black. H₂¹⁸O: Red. 1:1 H₂¹⁶O: H₂¹⁸O: Blue. b) Resonance Raman spectra of **3- α** (λ_{ex} 514.5 nm, 140 mW) prepared upon addition of 9 eq. of CAN to a 6 mM solution of **1- α** in 1:1 H₂O:MeCN. 1:1 H₂¹⁶O: H₂¹⁸O: Red. Sum of individual H₂¹⁶O and H₂¹⁸O spectra divided by 2: black.



Supplementary Figure 33. Resonance Raman with deuterated water. Resonance Raman spectra of **3- α** (λ_{ex} 514.5 nm, 140 mW) prepared upon addition of 9 eq. of CAN to a 6 mM solution of **1- α** in 1:1 H₂O:MeCN. H₂O: Black D₂O: Red.



Supplementary Figure 34. Ball and stick models. Top) Ball and stick models obtained from the XRD structures of **1-β** (left) and **1-α** (right). Bottom) Molecular Mechanics models of **3-β** (left) and **3-α** (right).

Supplementary Table 1. Determination of K_{eq} by the iterative method. Values for $\epsilon(2-\alpha)$ and $\epsilon(3-\alpha)$ at the different wavelengths obtained after the iterative determination of K_{eq} . This analysis provides a self-consistent value of $K_{eq} = 120 \text{ M}^{-1}$ that implies 17 % of **3- α** at 2.5 eq of CAN.

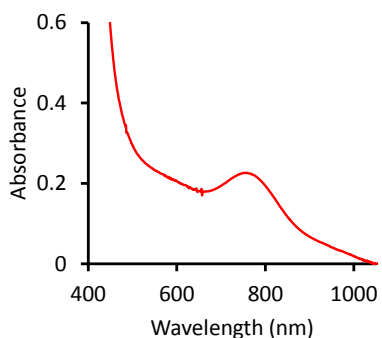
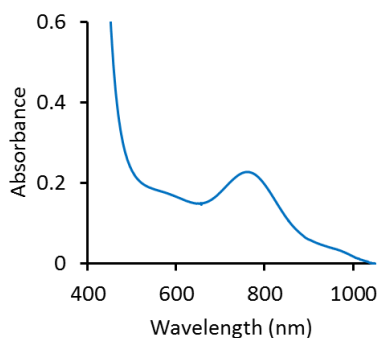
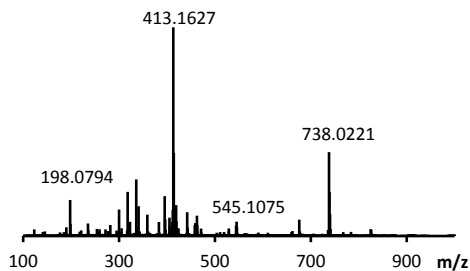
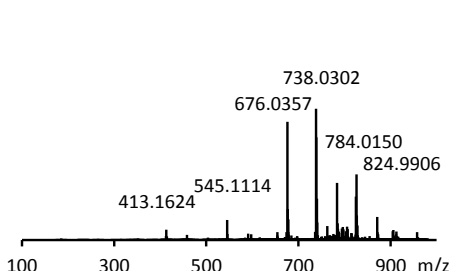
Wavelength (nm)	550	600	650	700	750	800
$\epsilon(2-\alpha)$	49	40	43	100	181	172
$\epsilon(3-\alpha)$	294	229	198	210	250	207
$\epsilon(2-\alpha)$ self-consistent calculated	-2	1	10	77	165	165
$\epsilon(3-\alpha)$ self-consistent calculated	305	237	205	215	253	209

Supplementary Table 2. Determination of the amount of 3- α for different K_{eq} values.

Relative amount of 3- α generated after addition of 2.5, 3 and 9 eq of CAN considering both $K_{eq} = 100$ and 140 M^{-1} . The analysis provides an improved K_{eq} value (120 ± 20).

K_{eq}	% 3- α		
	2.5 eq CAN	3 eq CAN	9 eq CAN
100	15	27	76
120	17	30	79
140	18	32	81

Supplementary Table 3. Summary of 3- α characterization under the two different conditions used in this paper. 20 mM of CAN and 1 mM of **1 α** were used in both cases.^[a] To obtain a good signal-to-ratio in the rR experiments, the concentrations of the complex and the oxidant used were 5 mM and 45 mM, respectively.^[b] At 75 mM of CAN concentration, yield of O₂ produced reaches 90 ± 8 %. The HRMS peak at 676.0282 m/z corresponds to the loss of neutral NO₃ from **3- α** . Peaks prominent at 784.0150 and 824.9906 m/z correspond to [**3- α**]+NO₃-O and [**3- α**]+NO₃+CN₃CN-O, respectively.

	Catalytic conditions (25 °C, H ₂ O)	at -8 °C in 1:1 MeCN:H ₂ O
UV-Vis		
ESI-MS		
rRaman^[a]	Measurement not possible	H ₂ ¹⁶ O: 677 cm ⁻¹ , 822 cm ⁻¹ H ₂ ¹⁸ O: 643 cm ⁻¹ , 782 cm ⁻¹
Yield of O₂ evolved	75 ± 5 % ^b	20 ± 2 %

Supplementary Methods

1. Titration of **2- α** with Ce^{IV}. Determination of the Fe^{IV}-Ce^{IV} binding constant.

In order to determination of the Ce^{IV} binding constant ($K_{eq} = [\mathbf{3-}\alpha] / ([\mathbf{2-}\alpha] \cdot [\text{Ce}^{\text{IV}}])$) to **2- α** , to form **3- α** we have titrated **2- α** with CAN and the obtained UV-Vis spectroscopic data at different wavelengths (550, 600, 650, 700, 750 and 800 nm) it was analyzed through fitting it to the mathematical expression used for the linearization of a **A + B = C** equilibrium as a function of $[\text{Ce}^{\text{IV}}]_0$, $[\mathbf{2-}\alpha]_0$ and $[\mathbf{3-}\alpha]$ where the K_{eq} is the slope of the expression: $(\gamma^{-1} - 1)^{-1} = K_{eq} \cdot ([\text{Ce}^{\text{IV}}]_0 - [\mathbf{3-}\alpha])$, (where $\gamma = [\mathbf{3-}\alpha] / [\mathbf{2-}\alpha]_0$). For mathematical demonstration of the K_{eq} expression, please see the following references: *J. Am. Chem. Soc.*, **2013**, *135*, 9186–9194; *J. Chem. Soc Perkin Trans. II*, **1989**, 1753-1761. Detailed information about the model fitting is provided bellow.

The titration experiments were carried out using a freshly prepared **2- α** by reaction **1- α** with minimum amount of Ce^{IV} (2.5 eq) to ensure the full formation of **2- α** . The need for 2.5 equivalents of Ce^{IV} to fully transform **1- α** into **2- α** is an indication of the high redox potential needed to oxidize the Fe^{III}-OH₂ to Fe^{IV}(O) species. Taking into consideration the Nernst equation the red-ox potential for the Fe^{III}-OH₂/Fe^{IV}(O) couple (under the low pH of the reaction conditions) it is estimated at ~ 1.4 V vs NHE, which matches that obtained in recent DFT calculations. Indeed, attempts to form **2- α** with lower amounts (2-2.4 eq) were not as fruitful. Absorbances were measured after (0-10 s) the addition of Ce^{IV} to **2- α** solutions. Absorbance values of the titrations range from 5 to 240 mM and were obtained by were obtained by triplicate.

2. Calculation of K_{eq} by UV-Vis spectroscopy.

We have calculated the K_{eq} by using an iterative self-consistent method. The method solves the contamination of the ϵ values for **2- α** and **3- α** . The method is described in the following lines.

The value of K_{eq} was calculated with the following expression:

$$K_{eq} = \frac{x}{(2\alpha - x)(Ce - x)} \quad (1)$$

Where x is the amount of product generated and, **2- α** and Ce are the initial concentrations of the reactants (**2- α** = 0.005 M, Ce = 0.0025 - 0.24 M (2.5 – 50 eq respect to **2- α**)).

A theoretical Ce-titration curve can be plotted as a function of K_{eq} by solving the 2nd degree equation. Where x is the concentration of **3- α** for the different Ce^{IV} concentrations and it can be expressed as a % of **3- α** respect to the $[\mathbf{2-}\alpha]_0$ ($[\mathbf{2-}\alpha]_0$ stands for the initial concentration of

Fe^{IV}=O). The % of **3-α** were normalized to directly compare the theoretical values with the experimental titration curves. The initial value of K_{eq} was guessed, and afterwards the K_{eq} value is calculated by an iterative self-consistent method.

As the reviewer pointed us, from this plot we can obtain the % of **2-α** and **3-α** at any concentration of Ce as a function of the K_{eq} value.

An absorbance (Abs (y)) resulting from a mixture of 2 species (species A and B) can be expressed as:

$$\text{Abs}(\mathbf{y}) = n \cdot \text{Abs}(\mathbf{A}) + m \cdot \text{Abs}(\mathbf{B}) \quad (2)$$

where n and m are % values (n+m = 100), and A and B are **2-α** and **3-α** respectively.

Abs (**3-α**) and Abs (**2-α**) can be obtained by solving a two-equation system. Therefore, the use of two different measures of Abs(y) at different concentrations of CAN will give us the values for Abs (**3-α**) and Abs (**2-α**), by using the expression **Eq.2**.

The n and m values in the **Eq.2** can be expressed as %(**3-α**)_x and %(**2-α**)_x, respectively where x is the used CAN equivalents. For convenience, 2.5 and 50 CAN equivalents were employed together with K_{eq} guessed in the expression **Eq.2**.

$$\text{Abs}_{2.5} = \%(\mathbf{3-}\alpha)_{2.5} \cdot \text{Abs}(\mathbf{3-}\alpha) + \%(\mathbf{2-}\alpha)_{2.5} \cdot \text{Abs}(\mathbf{2-}\alpha) \quad (3)$$

$$\text{Abs}_{50} = \%(\mathbf{3-}\alpha)_{50} \cdot \text{Abs}(\mathbf{3-}\alpha) + \%(\mathbf{2-}\alpha)_{50} \cdot \text{Abs}(\mathbf{2-}\alpha) \quad (4)$$

By solving the system, we obtain the values of Abs (**2-α**) and Abs (**3-α**).

$$5\text{Abs}(\mathbf{3-}\alpha) = \frac{\%(\mathbf{2-}\alpha)_{2.5} \cdot \text{Abs}_{50} - \%(\mathbf{2-}\alpha)_{50} \cdot \text{Abs}_{2.5}}{\%(\mathbf{2-}\alpha)_{2.5} \cdot \%(\mathbf{3-}\alpha)_{50} - \%(\mathbf{2-}\alpha)_{50} \cdot \%(\mathbf{3-}\alpha)_{2.5}} \quad (5)$$

$$\text{Abs}(\mathbf{2-}\alpha) = \frac{\text{Abs}_{2.5} - \%(\mathbf{3-}\alpha)_{2.5} \cdot \text{Abs}(\mathbf{3-}\alpha)}{\%(\mathbf{2-}\alpha)_{2.5}} \quad (6)$$

Once determined the initial Abs (**2-α**) and Abs (**3-α**) values, we calculated ε(**2-α**) and ε(**3-α**) (Beer-Lambert law, A = ε·l·c).

This was the first iteration of the self-consistent calculation method for the K_{eq}. At that point we have calculated the initial values for the K_{eq}, ε(**2-α**) and ε(**3-α**).

Now a value for the K_{eq} can be obtained by using the $\epsilon(2-\alpha)$ and $\epsilon(3-\alpha)$ and considering, $(\gamma^{-1}-1)^{-1}$ vs $[Ce^{IV}]_0-[3-\alpha]$ plot. At this point is important to remember that $\gamma = [3-\alpha] / [2-\alpha]_0$ and the slope of the $(\gamma^{-1}-1)^{-1}$ vs $[Ce^{IV}]_0-[3-\alpha]$ plot correspond to the K_{eq} .

Because the calculation of the K_{eq} and the molar absorptivity are connected between one to each other, we used an iterative GRG Nonlinear algorithm included in the “Solver” macro of MSExcel software package to self-consistent refining of the K_{eq} , $\epsilon(2-\alpha)$ and $\epsilon(3-\alpha)$ values. For the iteration, we have kept a high square correlation coefficient ($r^2 > 0.9$) for the $(\gamma^{-1}-1)^{-1}$ vs $[Ce^{IV}]_0-[3-\alpha]$ plots, while minimize the sum of the squared differences between the experimental titration absorbance values (average of 550 – 700 nm) and the theoretical values obtained by the K_{eq} . The method converged with a K_{eq} of $120 M^{-1}$.

After iterative determination of K_{eq} , values for $\epsilon(2-\alpha)$ and $\epsilon(3-\alpha)$ at the wavelengths can be found in Supplementary Table 1.

This analysis provides a self-consistent value of $K_{eq} = 120 M^{-1}$ that implies 17 % of $3-\alpha$ at 2.5 eq of CAN (the table below shows the amount of $3-\alpha$ generated after addition of 2.5 and 9 eq of CAN considering both $K_{eq} = 100$ and $140 M^{-1}$ (Supplementary Table 2). The analysis provides an improved K_{eq} value (120 ± 20) without affecting the conclusions of the manuscript.

3. HRMS isotopic pattern analysis.

HRMS of intermediate $3-\alpha$ presents a prominent peak at m/z 738.0235 (M_3) which shows a complex isotopic pattern. First of all, the experimental m/z obtained matches the m/z value calculated for the formulation of $3-\alpha$ as $\{[Fe^{IV}(O)(mcp)(\mu-O)Ce^{IV}(NO_3)_3]\}^+$ with an error lower than 1.5 ppm (calc. 738.0245 m/z). The individual peak separations for this peak cluster were found to be $m/z \pm 1$, indicating a mono-charged positive ion. Further information was gained by taking a closer look at its isotopic distribution pattern. The isotopic pattern related to the prominent peak at m/z 738.0235 (M_3) can be only correctly described by taking into account the natural isotopic distribution and abundance of both the Fe and the Ce atoms (Figure SI.14A). For instance the peak at m/z $M_3 - 2$ (736.0244) accounting for 6.5% of the M_3 peak, is indicative of the presence of one iron atom (isotopes and natural abundance of iron: 53.9, 5.8%; 55.9, 91.8%; 56.9, 2.1% and 57.9, 0.3%) in the molecule (Figure SI.14B). However, m/z 739.0274 and 740.0283 peaks are experimentally more intense than expected according to the simulation, suggesting the presence of some amount of Fe(III)-OH (the presence of Fe(III)-OH was also observed in the spectra of $2-\alpha$). Taking into account the presence of 16 % of Fe(III)-OH, peak at 739.0274 reaches its expected intensity (Figure SI.14C). In addition, peaks at 740.0283 and 741.0305 have lower intensities than expected if only the 139.9 cerium isotope is taking into

account. By taking into account the natural abundance of cerium (isotopes and natural abundance of cerium 135.9, 0.2%; 137.9, 0.2%; 139.9 88.45% and 141.9, 11.1%) these peaks match the isotopic pattern in the experimental spectrum, indicating the presence of this element in the formulation of **3- α** (Figure SI.14D).

Supplementary References

1. M. Costas, J. Que, L., Ligand Topology Tuning of Iron-Catalyzed Hydrocarbon Oxidations. *Angew Chem. Int. Ed.* **41**, 2179-2181 (2002).
2. M. Costas, A. K. Tipton, K. Chen, D.-H. Jo, L. Que, Modeling Rieske Dioxygenases: The First Example of Iron-Catalyzed Asymmetric cis-Dihydroxylation of Olefins. *J. Am. Chem. Soc.* **123**, 6722-6723 (2001).
3. J. Lloret Fillol, Z. Codolà, I. Garcia-Bosch, L. Gómez, J. J. Pla, M. Costas, Efficient water oxidation catalysts based on readily available iron coordination complexes. *Nat Chem* **3**, 807-813 (2011).
4. Z. Codolà, I. Garcia-Bosch, F. Acuña-Parés, I. Prat, J. M. Luis, M. Costas, J. Lloret-Fillol, Electronic Effects on Single-Site Iron Catalysts for Water Oxidation. *Chemistry – A European Journal* **19**, 8042-8047 (2013).